AERODYNAMIC SIZE ASSOCIATIONS OF NATURAL RADIOACTIVITY
WITH AMBIENT AEROSOLS

MASTER

E. A. BONDIETTI, Environmental Sciences Division, Oak Ridge
National Laboratory, Oak Ridge, TN 37831

C. PAPASTEFANOU, Nuclear Physics Department, Aristotle
University of Thessaloniki, Thessaloniki 540 06 Greece

C. RANGARAJAN, Division of Radiological Protection, Bhabha
Atomic Energy Research Centre, Trombay, Bombay 400 085, India

The aerodynamic size distributions of Pb-214, Pb-212, Pb-210, Be-7, P-32, S-35 (as SO_4^{2-}), and stable SO_4^{2-} were measured using cascade impactors. The activity distribution of Pb-212 and Pb-214, measured by alpha spectroscopy, was largely associated with aerosols smaller than 0.52 μm. Based on 46 measurements, the activity median aerodynamic diameter of Pb-212 averaged 0.13 μm (σ_g = 2.97), while Pb-214 averaged 0.16 μm (σ_g = 2.86). The larger median size of Pb-214 was attributed to α-recoil depletion of smaller aerosols following decay of aerosol-associated Po-218. Subsequent Pb-214 condensation on all aerosols effectively enriches larger aerosols. Pb-212 does not undergo this recoil-driven redistribution. Low-pressure impactor measurements indicated that the mass median aerodynamic diameter of SO_4^{2-} was about three times larger than the activity median diameter of Pb-212, reflecting differences in atmospheric residence times as well as the differences in surface area (Pb-212) and volume (SO_4^{2-}) distributions of the atmospheric aerosol. Cosmogenic radionuclides, especially Be-7, were associated with smaller aerosols than SO_4^{2-} regardless of season, while Pb-210 distributions in summer measurements were similar to sulfate but smaller in winter measurements. Even considering recoil following Po-214 α-decay, the average Pb-210-labeled aerosol grows by about a factor of two during its atmospheric lifetime. The presence of 5 to 10% of the Be-7 on aerosols greater than 1 μm was indicative of post-condensation growth, probably either in the upper atmosphere or after mixing into the boundary layer.

The decay of Rn-222 and Rn-220 in the atmosphere produces low vapor pressure progeny that coagulate with other nuclei or condense on existing aerosols. These progeny include 3.0-min (radioactive half-life) Po-214, 26.8-min Pb-214, and 10.6-h Pb-212. A long-lived daughter in the Rn-222 decay chain, 22-year Pb-210, is produced about an

hour after attachment of Po-218. Cosmic ray bombardment of gases in the atmosphere also produces condensable radionuclides. For example, N_2 and O_2 are percursors of 53.3-d Be-7, and Ar-40 gives rise to 87-d S-35 and 14-d P-32. The atmospheric residence times of these radionuclides are controlled either by radiodecay or aerosol removal.

In addition to these nuclear reactions, myriads of other gas-phase transformations produce low-vapor pressure species, with the oxidation of SO_2 and other reduced sulfur species dominating aerosol formation and growth. Oxidation of SO_2 in the gas phase produces H_2SO_4, a readily condensable species that either combines with other molecules (new particle formation) or condenses on existing aerosols.

While condensational growth is principally responsible for aerosol growth up to several tenths of a micron (Hering and Friedlander, 1982; McMurray and Wilson, 1983), oxidation of SO_2 also occurs in the aerosol phase through chemical reactions. This model of SO_2 oxidation is believed to be responsible for growth of aerosols above several tenths of a micron (Hering and Friedlander, 1982; McMurray and Wilson, 1983), because growth rates increase with aerosol diameter, in contrast to condensational growth, where diameter growth decreases as diameter increases (Friedlander, 1977).

Aerodynamic Size Distributions of Naturally-Radioactive Aerosols. Measurements of radionuclide distributions using cascade impactors indicate that Be-7 and Pb-210 are associated with larger aerosols than Pb-212 and Pb-214 (Röbig et al., 1980; Papastefanou and Bondietti, 1986). Measurements of Pb-210 associations over oceans indicated activity median aerodynamic diameters (AMAD) near 0.6 μm (Sanak et al., 1981). The impactor measurements of Moore et al. (1980) on Pb-210, Bi-210, and Sr-90 sizes in continental air indicated that about 80% of the activity from all three nuclides was associated with aerosols below 0.3 μm. That work also determined that the mean age of aerosol Pb-210 was about a week. Knuth et al. (1983) compared Pb-210 and stable Pb sizes at a continental location and found that 78% of the Pb-210 found below 1.73 μm was smaller than 0.58 μm. Young (1974) reported that the most of the Be-7 in the atmosphere was associated with submicron aerosols.

This paper summarizes part of the results of an investigation designed to characterize the aerodynamic size distributions of natural radioactivity and to evaluate the results in the context of sulfate distributions and recent advances in the understanding of aerosol growth mechanisms. This paper, while emphasizing our results of Pb-212 and Pb-214, also summarizes our initial data for longer-lived radionuclides.

Experimental Methods

Measurements on aerodynamic sizes of atmospheric aerosols and associated radionuclides were carried out with Anderson 2000, Inc., 1-ACFM cascade impactors with or without the Anderson low-pressure modification, as well as with Sierra model 236 (six-stage) high-volume impactors (HVI). The 1-ACFM design operated at 28 L min^{-1} (1 ft^3 min^{-1}). The stages had effective cutoff diameters (ECDs) of 0.4, 0.7, 1.1, 2.1, 3.3, 4.7, 7.0, and 11.0 μm. The low-pressure modification, which alters the impactor's operation by increasing the resolution in the submicron region, involves a regulated flow rate of 3 L min^{-1}, five low-pressure

(114 mm Hg) stages for the submicron region and eight atmospheric pressure stages for separating aerosols above 1.4 μm. The ECDs of the low-pressure stages were 0.08, 0.11, 0.23, 0.52, and 0.90 μm, whereas for the upper stages they were 1.4, 2.0, 3.3, 6.6, 10.5, 15.7, 21.7, and 35.0 μm. The stainless steel plates supplied by the manufacturer were used for aerosol collection. Either polycarbonate or glass-fiber backup filters were used to collect all particles below the 0.08-μm collection plate. The Sierra HVI had ECDs of 0.41, 0.73, 1.4, 2.1, 4.2, and 10.2 μm. All impactors were operated at the flow rates and pressures specified in the manufacturers' operating manuals, and collection occurred directly on the impactor stages.

The length of each collection period varied from about 3 h for Pb-214, to 30 or 40 h for Pb-212 and 1 to 14 d for Be-7, Pb-210, S-35, and P-32, depending on impactor and objective. The samples were collected 13 m above the ground on the roof of the Environmental Sciences Division building, Oak Ridge National Laboratory.

The deposits on the stainless-steel collection plates of the low-pressure impactor (LPI) were leached with a solution of $\underline{M}$ HNO_3 and the leachate rapidly evaporated on 5.08-cm stainless steel plates (using a hot plate). The concentrations of Pb-212 and Pb-214 in the impactor plate leachates were measured using seven ZnS(Ag) alpha scintillation counters.

The HVI plates were leached with 0.1 $\underline{M}$ HCl. Be-7 was measured using intrinsic germanium coaxial and well detectors. Lead-210 was determined 30 days after collection stopped by separating and measuring Bi-210 (Poet et al., 1972). When Pb-210 was measured, the upper two HVI stages were coated with a thin layer of petroleum jelly to minimize soil particle bounce.

Sulfur-35 was measured by purifying the sulfate from the HVI leachates using an alumina column (Veljkovic and Milenkovic, 1958). After eluting the sulfate from the alumina column with NH_4OH, it was converted to H_2SO_4 using a small Dowex-50(H^+) column. The resulting solution of dilute sulfuric acid was concentrated and the β-activity determined using liquid scintillation techniques. The purity of S-35 was checked by following the decay rate of the isolated β-activity. Phosphorus-32 was isolated from $\underline{M}$ HCl by precipitation of zirconium phosphate (Mullins and Leddicotte, 1962). Nonradioactive sulfate was determined by Dionex anion-exchange chromatography methods.

While nucleopore polycarbonate membranes (0.4 μm) were preferred as backup filters when sulfate was to be measured, glass-fiber filters had to be used in the HVI measurements. Because of potential glass fiber sulfate artifacts, a separate sampling for total sulfate was made using a polycarbonate filter.

Results

Pb-214 and Pb-212 Distributions.

The α-activity recovered from the LPI stages initially decayed at a 26.8-min half-life (i.e., Pb-214); after three hours, the rate approached that of 10.6-h Pb-212 (Papastefanou and Bondietti, 1986). The measured alphas were actually derived from the daughters of these nuclides. The counting rate data were analyzed by differential decay rate analysis after background correction to determine the Pb-214 and Pb-212 activity of the samples at the stop sampling time. The 1 σ counting uncertainties were 5% or less for stages corresponding to aerosols below 0.52 μm and <15% for the stages collecting aerosols above 0.52 μm. The calculated

activities of Pb-214 and Pb-212 were then used to determine the activity size distribution of each radionuclide. Po-218 does not directly contribute alpha particles during the measurements because of the long sampling time (>3 h) and the 15-min minimum delay between the sampling stopped and the time counting began. Alphas from Pb-210 and other nuclides were negligible as confirmed by repeated examination of the count rates after the normal 24-h recording period.

The observed activity size distributions of Pb-214 and Pb-212 vs aerodynamic diameter (D_p) are represented by the four subplots in Figure 1. These distributions were selected from 46 measurements made over a ten-month period (Papastefanou and Bondietti, 1986). About 46% of the measurements showed a radioactivity peak in the 0.11- to 0.23-μm region (subplot a), while 39% showed a peak in the 0.23- to 0.52 μm region (subplot b). The remaining 15% of the measurements resulted in distributions similar to those in subplot c (8.7%) or d (6.5%), where Pb-214 and Pb-212 activities were highest in different size ranges in the same spectrum. On the average about 76% of th Pb-214 activity and ≤7% of the Pb-212 activity was found to be associated with aerosols in the 0.08- to 1.4-μm size range. The activity associated with aerosols smaller than 0.8-μm can also be substantial, as indicated in Figure 1.

Table I presents the average aerodynamic distributions of Pb-212 and Pb-214, as well as the frequency with which Pb-214 or Pb-212 was the dominant isotope in each size range. The Aitken nuclei fraction (below 0.08 μm) contained a higher percentage of Pb-212 activity compared with Pb-214 in 69.6% of the measurements. The predominance of Pb-212 in this fraction is also illustrated by the distributions reported in Figure 1. In the remaining measurements, where Pb-214 was fractionally more abundant below 0.08 μm, the disparity between the relative amounts of each isotope was not nearly as dramatic. Conversely, Figure 1 and Table I illustrate that Pb-214 is generally enriched in the accumulation mode aerosol, particularly between 0.11 and 0.52 μm, where most of the surface area and mass occurs.

The shift of Pb-214 to a slightly higher size distribution compared to Pb-212 was also found using 1-ACFM and HVI impactors (Fig. 2). The higher flow rates of these impactors, as well as the ability to measure HVI activity by gamma spectroscopy, made us confident that this shift was real and not a data analysis artifact.

The Pb-214 AMADs, determined with the LPI, varied from 0.10 to 0.37 μm (mean value, 0.16 μm). For Pb-212, they varied from 0.07 to 0.245 μm (mean value 0.12 μm) (Papastefanou and Bondietti, 1986). These AMAD calculations were made assuming lognormal distributions. An abbreviated version of these results is presented in Table II.

Pb-212 vs SO_4^{2-} LPI Distributions. Figure 3 presents a summary of the average Pb-212 AMADs and SO_4^{2-} MADs (mass median aerodynamic diameters) determined from a series of LPI measurements made during the period January to October, 1985. The Pb-212 data were derived from collections made at the same time as SO_4^{2-} and from measurements made to compare Pb-212 vs Pb-214. The mean aerodynamic diameter of Pb-212 was about three times smaller than SO_4^{2-}. Much less sulfate was found in the aerosol fraction below 0.08 μm, compared with Pb-212. While Pb-212 was largely absent above 0.52 μm, about 20% of the SO_4^{2-} occurred above this size.

Be-7, Pb-210, S-35, P-32 and SO_4^{2-}. The longer-lived radionuclides were associated with larger aerosols than Pb-214 or Pb-212. An example of these differences is presented by Figure 4, which compares the distribution of Pb-212, Pb-210, SO_4^{2-}, Be-7, S-35, and P-32 found on two-six stage HVIs operated continuously for one week in February, 1985. Figure 4 illustrates that Pb-210, the cosmogenic radionuclides, and SO_4^{2-} were associated with larger aerosols than Pb-212. In most of our analyses, the fraction of Be-7 associated with aerosols above 1.4 µm was usually between 5 and 10%; in this measurement 4.5% was found in the 1.4 to 2.1 µm size range, 1.1% in the 2.1 to 4.2 µm size range, and only 0.2% in sizes greater than 4.2 µm. Figure 4 also shows that cosmogenic S-35, measured as SO_4^{2-}, does not have the same aerosol distribution as stable SO_4^{2-}; this same result occurred in two other measurements. The abundance of S-35 above 1.4 µm is unknown; the S-35 and P-32 distributions presented in Figure 4b (as well as the Pb-210 distributions in Figure 4a) represent only the three collection stages below 1.4 µm, due to a current limitation in the detection of low concentrations of these beta-emitters.

Table III summarizes the median aerodynamic diameters of Pb-210, Be-7, and SO_4^{2-} found in measurements made through March 1986. Be-7 distributions are substantially smaller than SO_4^{2-}, regardless of the time of the year. The Pb-210 data, while limited, suggests that summer sizes are larger than winter sizes.

Pb-210 vs Pb-214 Distributions. Pb-210 is produced from the α-decay of Po-214, the event used to quantify Pb-214 distributions on the HVI impactors. While the relationship between the aerodynamic sizes of Po-214 and Pb-210 is complicated because of the large differences in their atmospheric lifetimes, Pb-210 has always been found associated with aerosols larger than Po-214, as indicated by the differences in AMADs reported in Tables II and III.

Discussion

Alpha-Recoil: An Explanation for the Pb-214 Distributions. The longer half-life of Pb-212 compared to Pb-214 might favor the presence of larger aerosol associations of Pb-212 if coagulation rates are fast relative to radioactive decay rates, although impactor measurements may not be sensitive enough to record this effect. Instead, the measurements indicated that the shorter-lived chain (Po-218, Pb-214, etc.) was more often associated with larger aerosol sizes than the longer-lived chain (Po-216, Pb-212, etc.). The HVI measurements reported by Röbig et al. (1980) also indicated a large particle shift of Pb-214 relative to Pb-212, although they did not offer an explanation for the observation.

The Pb-214 shift might be explained by the fact that a significant fraction of the 3.05-min parent of Pb-214 should attach to an existing aerosol or coagulate with other nuclei during its lifetime, as mean attachment half-lives are the order of a minute less (Pörstendorfer and Mercer, 1980). When this attached Po-218 α-decays, the recoiling Pb-214 daughter can escape the aerosol. Complete recoil loss would occur if the diameter of the aerosol were smaller than the range of the recoiling nucleus. In water this recoil range is 0.13 µm (Mercer, 1976) and should be somewhat less in the atmospheric aerosol that has a density closer to 1.5 g cm^{-3} (Herring and Friedlander, 1982). By

contrast, very little of the 0.146 μs Po-216 would attach before decaying to Pb-212 because of its short life relative to attachment times. A considerable fraction of the Pb-214 should undergo recoil detachment, particularly from aerosols with diameters smaller than 0.1 μm (diameters approximating the recoil range). The probability of loss would decrease with increasing radius (Mercer, 1976). If the recondensing Pb-214 behaves like the original Po-214, the net effect would be a shift of Pb-214 to a larger size distribution.

Since the subsequent β-decays of Pb-212 and Pb-214 + Bi-214 do not result in significant recoil (Mercer, 1976), the alpha measurement of Po-214 and the Pb-212 daughters is in reality tracing the aerosol distribution of a Rn-220 daughter atom (Pb-212) which has condensed only once and a Rn-222 daughter atom (Pb-214) that has probably condensed more than once. This stability of the Pb isotopes is the basis for our generic reference to Pb-212 and Pb-214 distributions.

A Recoil Model That Accounts for The Pb-214 Shift. The following equations describe an empirical model that outlines the hypothesis more formally. First, the radon daughters are defined in terms of their atmospheric distributions at some time during their life:

A = the fraction of the total Po-218 that attaches to any aerosol before it decays to Pb-214;

$1 - A$ = the fraction of the total Po-218 that decays before aerosol attachment;

R_i = the fraction of the Pb-214 that, through recoil, is lost from aerosol size interval i following [218]Po decay;

$1 - R_i$ = the fraction of Pb-214 that remains with aerosol size interval i following Po-218 decay;

f_i = fraction of the total unattached atoms (Po-218 or Pb-214) that condense on size interval i.

Then, it is assumed that f_i, the fractional distribution of condensing isotopes on size interval i, can be derived from the measured Pb-212 distributions (i.e., the half-life of Po-218 is short enough that the distribution of daughter Pb-212 represents the initial fate of condensing species).

For A, the fraction of the total Po-218 that attaches before decay, the recoiling daughter Pb-214 produced in any size interval can fractionate as follows:

$$Fe_i = Af_iR_i , \tag{1}$$

where Fe_i is the fraction of the total Po-218 atoms that result in recoiling Pb-214 atoms that escape size interval i, and

$$Fn_i = Af_i(1 - R_i) , \tag{2}$$

where Fn_i is the fraction of the total attached Po-218 atoms that result in recoiling Pb-214 atoms that do not escape size interval i. Summing all size intervals in terms of Equation (1) gives:

$$Fe_s = \sum_i A f_i R_i = A \sum_i f_i R_i , \qquad (3)$$

where Fe_s represents the sum of all Po-218 atoms that condense and then escape (as Pb-214) the atmospheric aerosol after decay.

Condensing Pb-214, while assumed to follow the same size distribution as observed for Pb-212, is derived from two sources which must be considered separately. First,

$$Fu_i = f_i(1-A) , \qquad (4)$$

where Fu_i is the fraction of the Pb-214 in size interval i that originated by condensation of Pb-214 that originated from the decay of Po-218 before condensation; and second,

$$Fd_i = f_i Fe_s , \qquad (5)$$

where Fd_i is the fraction of the total Pb-214 associated with size interval i that originated from the deposition of the Pb-214 that had escaped from all aerosol fractions (Fe_s) following decay of attached Po-218. These Pb-214 atoms, which originated by recoil detachment from the general aerosol population, are condensing for the second time. Because the probability of recoil detachment decreases with increasing aerosol diameter, the greater depletion of the smaller aerosols effectively results in a shift of the total Pb-214 atoms to a higher size distribution.

From the above definitions the total Pb-214 atoms can be accounted for as follows:

$$Ft_i = Fu_i + Fd_i + Fn_i, \qquad (6)$$

where Ft_i is the fraction of the total measured Pb-214 that occurs in size interval i. Summing Equation (6) for all size intervals gives:

$$Ft_s = \sum_i Ft_i. \qquad (7)$$

Equations 6 and 7 were solved for values of R_i and A that gave the best fit between observed and calculated Pb-214 distributions. The various impactor stages were used for deriving the size intervals. An example of the results of this model is presented in Figure 5. In this calculation, A was assumed to be 0.963 (i.e., 96.3% of the Po-218 was assumed to attach to ambient aerosols before decay to Pb-214). The best agreement between calculated and measured Pb-214 distributions was found for the case when calculated recoil losses (R_i) of 100, 70, 65, and 35% occurred from the < 0.11-, 0.11- to 0.23-, 0.23- to 0.52-, and 0.52- to 0.90-μm size ranges, respectively. In this example, the percentage

of the total Pb-214 that underwent recoil detachment was calculated to be 79.6%, very similar to values predicted in a theoretical analysis (Mercer, 1976) and calculated from experimental data obtained when atmospheric aerosols were exposed to an enriched radon atmosphere (Mercer and Stowe, 1971). In solving for the best fit between calculated and observed Pb-214 distributions, the <0.08-μm and 0.08- to 0.11-μm measurements were combined to improve the fit. This simplification was made because of (1) the low fractional contribution of the 0.08- to 0.11-μm region to the total activity, (2) the likelihood that recoil losses will approach 100% in this size region (Mercer, 1976), and (3) the possibility that coagulative growth of Pb-212 out of the < 0.08-μm region might be significant during its lifetime.

This model does not explicitly consider that a fraction of the measured Pb-214 actually deposits in the impactor as particle-associated Po-218. The Pb-214 daughters produced under this condition would either not recoil off the plate or, if they did, they might end up associated with a smaller size fraction on a lower stage. In terms of both the model and the measurements, this fraction of the total Po-218 is not operationally different from the fraction which decays before attachment (1-A) or is not lost following recoil; both represent Po-218 which does not undergo recoil redistribution.

Estimating Recoil Redistribution of Pb-210 Following Po-214
α-Decay. In addition to Pb-214, Pb-210 would also undergo α-recoil following decay of Po-214. Since the Po-214 is separated from Pb-214 by only β-decays, the model parameters derived above can be used to calculate the aerodynamic size distribution of Pb-210 that would result if condensation processes (and recoil) alone affect radioactivity sizes.

For the values of R_i derived previously (Figure 5), the amount of recoiling Pb-210 can be calculated using Equation 3, substituting the measured Pb-214 distribution (Table I) for f_i. The distribution of condensing Pb-210 can be derived from Equation 5, where Fd_i now represents the fraction of the total Pb-210 associated with size interval i that originated from Pb-210, which had escaped from all aerosol fractions following Po-214 decay. The calculated Pb-210 distributions, using this model, are: <0.11 μm, 31.7% (vs 32.7% for Pb-214; 0.11 to 0.23 μm, 26.2% (vs 27.4% for Pb-214); 0.23 to 0.52 μm, 30.8% (vs 30.5% for Pb-214; 0.53 to 0.9 μm, 5.1% (vs 4.1% for Pb-214); and 0.9 to 1.4 μm, 3.5% (vs 2.6% for Pb-214). The AMAD derived from this new Pb-210 distribution is 0.18 μm, substantially lower than actually measured, indicating that the presence of Pb-210 in larger aerosol sizes must result from post-condensation growth.

Pb-212 and SO_4^{2-} Distributions. The aerodynamic size distributions of Pb-212 and SO_4^{2-} were quite different, reflecting the different dependencies of surface area and volume on aerosol diameter (Friedlander, 1977). Pb-212, like the other radionuclides, becomes associated with the atmospheric aerosol by condensation or coagulation processes that are surface-area related. Sulfate, on the other hand, is the main solute in the accumulation mode aerosol so that its steady-state distribution is proportional to volume, even though condensation of H_2SO_4 may dominate its initial aerosol association. The difference also reflects residence time: 16.7 h for Pb-212 + Bi-212 and about a week for sulfate.

Pb-210 and the Cosmogenic Radionuclides. We noted earlier that our measurements of Pb-214 were really measurements of Po-214 decay, that is, the production of Pb-210. The mean AMAD of these measurements was about 0.16 μm, with the AMAD of Pb-210 predicted to be ~0.18 μm after recoil. However, the summer AMAD of Pb-210, after aging in the atmosphere for about a week (Moore et al., 1980), was closer to 0.4 μm, indicating that Pb-210's AMAD approximately doubles during its lifetime in the atmosphere. The limited measurements reported here suggest that the AMAD of Pb-210 is smaller in winter than summer, possibly reflecting differences in aerosol growth rates. The summer measurements were also not different from simultaneous SO_4^{2-} measurements.

The cosmogenic radionuclides, particularly Be-7, are associated with slightly smaller aerosols than sulfate, both in winter and summer. The reasons for this difference may be either (1) faster growth rates of secondary SO_4^{2-} aerosols in plumes from sources or (2) the direct contribution of primary sulfate aerosols from these sources. Coarse aerosol sulfate (above several μm) may be a factor in some cases. By contrast, the cosmogenic nuclides are produced in the stratosphere and upper troposphere and mix into the boundary layer with considerable week-to-week fluctuations (Rangarajan and Gopalakrishnan, 1970). While sizes distributions in the upper atmosphere have not been measured, artificial radioactivity from high-altitude nuclear tests was found associated with aerosols about 0.1 to 0.2 μm in size (Martell, 1962).

Radionuclide Sizes Relative to Growth Mechanisms
of Sulfate Aerosols. Hering and Friedlander (1982), in a study of the Los Angeles Basin sulfate aerosol, observed the occurrence of two categories of sulfate distributions: one with a mass median diameter of 0.54 ± 0.07 μm and one with a mass median diameter of 0.20 ± 0.02 μm. Based on a growth model, they concluded that condensational processes dominated the formation of the small distributions. At much higher sulfate loadings than found in our measurements (i.e., 11 μg m^{-3}, Figure 4), they concluded that coagulation times of several weeks were required to increase aerosol volume distributions from 0.25 to 0.50 μm. Because air masses have much shorter residence times in the Basin, they concluded that distributions near 0.5 μm were the result of rapid growth in the liquid phase.

McMurray and Wilson (1982; 1983) examined aerosol growth in urban plumes and remote locations and concluded that both condensation and droplet-phase reactions contributed to aerosol growth, with humidity and sunlight important variables. For example, an analysis of measurements on the St. Louis, Missouri, urban plume indicated that 75% of secondary aerosol volume formation was attributed to condensation and 25% to droplet-phase reactions. They further concluded that in humid climates, droplet-phase growth was responsible for the presence of submicron volume distributions peaking in the 0.3- to 0.5 μm-dia range; in arid climates the presence of submicron volume distributions, which peaked near 0.2 μm, was considered to be due to condensation-dominated growth.

Our measurements on radionuclide sizes can be evaluated in terms of these mechanisms, although the significance of droplet-phase growth remains uncertain. Lead-212 distributions reflect, of course, condensational growth. The rate at which mass (as Pb-212 atoms) deposits to the aerosol decreases with increasing diameter, as predicted

by the growth law (McMurray and Wilson, 1982). The Pb-214 distributions also reflect condensational growth but with the added complication of recoil. The oxidation rate of SO_2 is at a minimum during winter, affecting both the rate of new particle production and the growth of aerosols by chemical reactions in the liquid phase. Therefore, the growth of Pb-210 from less than 0.2 μm to slightly over 0.3 μm during the winter may establish a lower limit for growth by coagulation during the approximately one week Pb-210 resides in the atmosphere.

McMurray and Wilson (1982) calculated aerosol growth rates by determining the change in diameter (D_p) with respect to time. By analogy, the growth of Pb-210 in the atmosphere can be calculated by dividing the ~0.2 μm change in AMAD by the mean residence time of Pb-210. The resulting growth rate is approximately 0.001 μm h^{-1}, indicating growth by condensation or coagulation (McMurray and Wilson, 1982; 1983). We also conclude that the upper limit of aerosol growth is between 2 and 4 μm, as indicated by the Be-7 results. Additional insights into aerosol growth rates may be gained by evaluating the ages of Pb-210 on the 0.73- to 2.1-μm size range (stages 5 and 4 of the Sierra 236 HVI) using the Bi-210 in-growth method (Poet et al., 1972; Moore et al., 1980). Very little Pb-214 condenses in this size range so that the age of those fractions should reflect post-condensation growth aging. This approach may be especially useful during the summer when growth rates are fast. Measurements must be done in climates where soil resuspension is minimal, however, and the fractional distribution of Be-7 should be used as a guide for evaluating if Pb-210 distributions can be safely attributed to a condensation origin.

The rates and mechanisms of aerosol growth in the atmosphere are obviously quite complicated. Natural radionuclides are unique tracers in that they can show (1) where condensational growth is occurring (Pb-212), (2) the average growth rate that occurs from 0.2 to 0.4 μm during (Pb-210), and (3), how growth rates differ with respect to season and entry point into the mixed layer (Be-7 and Pb-210). The presence of Be-7 as a global tracer of aerosols mixing into the boundary layer also suggests that the influences of humidity, aerosol precursor concentrations, and other variables can be compared geographically. For example, we observed much larger Pb-210 aerosol sizes than reported by Moore et al. (1980) in Colorado. Is this a humidity or pollution effect or a methodology difference? Sanak et al. (1981) found larger Pb-210 aerosols in the marine boundary layer. Why? Was it because they used glass-fiber substrates on each impactor stage or do aerosols attain different sizes over the oceans? More systematic comparisons are obviously needed.

Summary

The aerodynamic size distributions of Pb-214, Pb-212, Pb-210, Be-7, P-32, S-35-SO_4^{2-}, and stable SO_4^- were measured using cascade impactors. Pb-212 and Pb-214, measured by alpha spectroscopy, were largely associated with aerosols small than 0.52 μm. Based on over 46 low-pressure impactor measurements, the mean activity median aerodynamic diameter (AMAD) of Pb-212 was found to be 0.13 μm, while for Pb-214 the AMAD was larger--0.16 μm. The slightly larger size of Pb-214, confirmed with operationally different impactors, was attributed to α-recoil-driven redistribution of Pb-214 following decay of

aerosol–associated Po–218. A recoil model was presented that explained this redistribution. Low-pressure impactor measurements indicated that the mass median aerodynamic diameter of SO_4^{2-} (0.38 μm) was about three times larger than the activity median diameter of Pb–212, reflecting differences in atmospheric residence times as well as the differences in surface area (Pb–212 and volume (SO_4^{2-}) distributions of the atmospheric aerosol. Cosmogenic radionuclides, especially Be–7 and S–35, were associated with smaller aerosols than SO_4^{2-} regardless of the time of year. Lead–210 distributions were similar to sulfate in summer measurements but smaller in winter measurements. Even considering recoil following Po–214 alpha decay, the average Pb–210–labelled aerosol grows by about a factor of two during its atmospheric lifetime. Five to ten percent of the Be–7 occurred on aerosols larger than 1 μm, indicating that post–condensational growth is significant.

References

Friedlander, S. K., Smoke, Dust, and Haze, John Wiley & Sons, Inc., New York, NY (1977).

Hering, S. V., and S. K. Friedlander, Origins of Aerosol Sulfur Size Distributions in the Los Angeles Basin, Atmos. Environ. 11:2647-2656 (1982).

Knuth, R. H., E. O. Knutson, H. W. Feely, and H. L. Volchock, Size Distributions of Atmospheric Pb and Pb-210 in Rural New Jersey: Implications for Wet and Dry Deposition, in Precipitation Scavenging, Dry Deposition, and Resuspension, Vol. 2, pp. 1325-1336, Elsevier Science Publishers (1983).

Martell, E. A., The Size Distribution and Interaction of Radioactive and Natural Aerosols, Tellus, 18:486-498 (1962).

McMurray, P. H. and J. C. Wilson, Droplet Phase (Heterogeneous) and Gas Phase (Homogeneous) Contributions to Secondary Ambient Aerosol Formation As Functions of Relative Humidity, Atmos. Environ., 16(1):121-134 (1982).

McMurray, P. H. and J. C. Wilson, Growth Laws for the Formation of Secondary Ambient Aerosols: Implications for Chemical Conversion Mechanisms, J. Geophy. Res., 88(C9):5101-5108 (1983).

Mercer, T., The Effect of Particle Size on the Escape of Recoiling RaB Atoms from Particulate Surfaces, Health Phys. 31:173-175 (1976).

Mercer, T. and W. A. Stowe, Radioactive Aerosols Produced by Radon in Room Air, in Inhaled Particles II, The Gresham Press, Surry, England (1971).

Moore, H. E., S. E. Poet and E. A. Martell, Size Distributions and Origin of Pb-210, Bi-210, and Po-210 on Airborne Particles in the Troposphere, in Natural Radiation Environment III, (T. F. Gesell and W. M. Lowder, eds.), CONF-780422, Vol, 1, pp. 415-429, National Technical Information Service, Springfield, Virginia (1980).

Mullins, W. T. and G. W. Leddicotte, The Radiochemistry of Phosphorus, NAS-NS 3056, National Technical Information Service, Springfield, Virginia (1962).

Papastefanou, C. and E. A. Bondietti, Aerodynamic Size Associations of Pb-212 and Pb-214 in Ambient Aerosols, submitted to Health Phys. (1986).

Poet, S. E., H. E. Moore and E. A. Martell, Lead-210, Bi-210, and Polonium-210 in the Atmosphere: Accurate Ratio and Application to Aerosol Residence Time Determination, J. Geophys. Res., 77:6515-6527 (1972).

Porstendörfer, J. and T. Mercer, Diffusion Coefficient of Radon Decay Products and their Attachment Rate to the Atmosphere Aerosol, in Natural Radiation Environment III, (T. F. Gesell and W. M. Lowder, eds.), CONF-780422, Vol. 1, pp. 281-293, National Technical Information Service, Springfield, Virginia (1980).

Rangarajan, C. and S. S. Gopalakrishnan, Seasonal Variation of Beryllium-7 Relative to Cesium-137 in Surface Air at Tropical and Subtropical Latitudes, Tellus 22:115-120 (1970).

Röbig G., K. H. Becker, A. Hessin and J. Porstendörfer in Proc. 8th Conference on Aerosol Sci., pp. 96-102, George-August-University, Gottingen, West Germany (1980).

Sanak, J., A. Gaurdy and G. Lambert, Size Distributions of Pb-210 Aerosols over Oceans, Geophys. Res. Lett., 8(10):1067-1070 (1981).

Veljkovic, S. R., and S. M. Milenkovic, Concentration of Carrier-free Radioisotopes by Adsorption on Alumina, in Proc. of the 2nd UN Conference on Peaceful Uses of Atomic Energy. Vol. 20, pp. 45-49, United Nations (1958)

Young, J. A., The Particle Size Distribution of Man-made and Natural Radionuclides, in Pacific Northwest Laboratory Annual Report for 1973, Part 3, pp. 16-17 (atmospheric sciences), Richland, Washington, (1974).
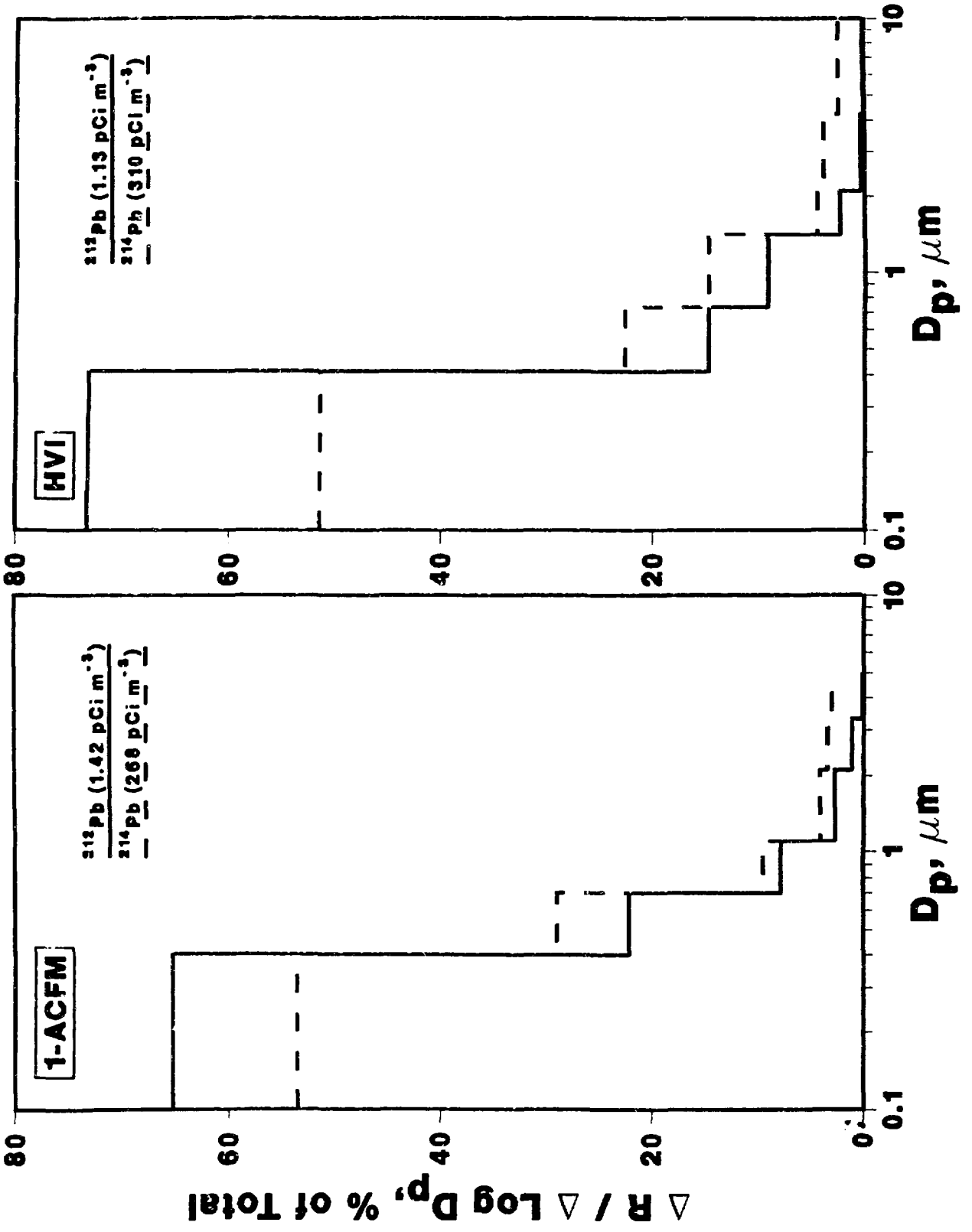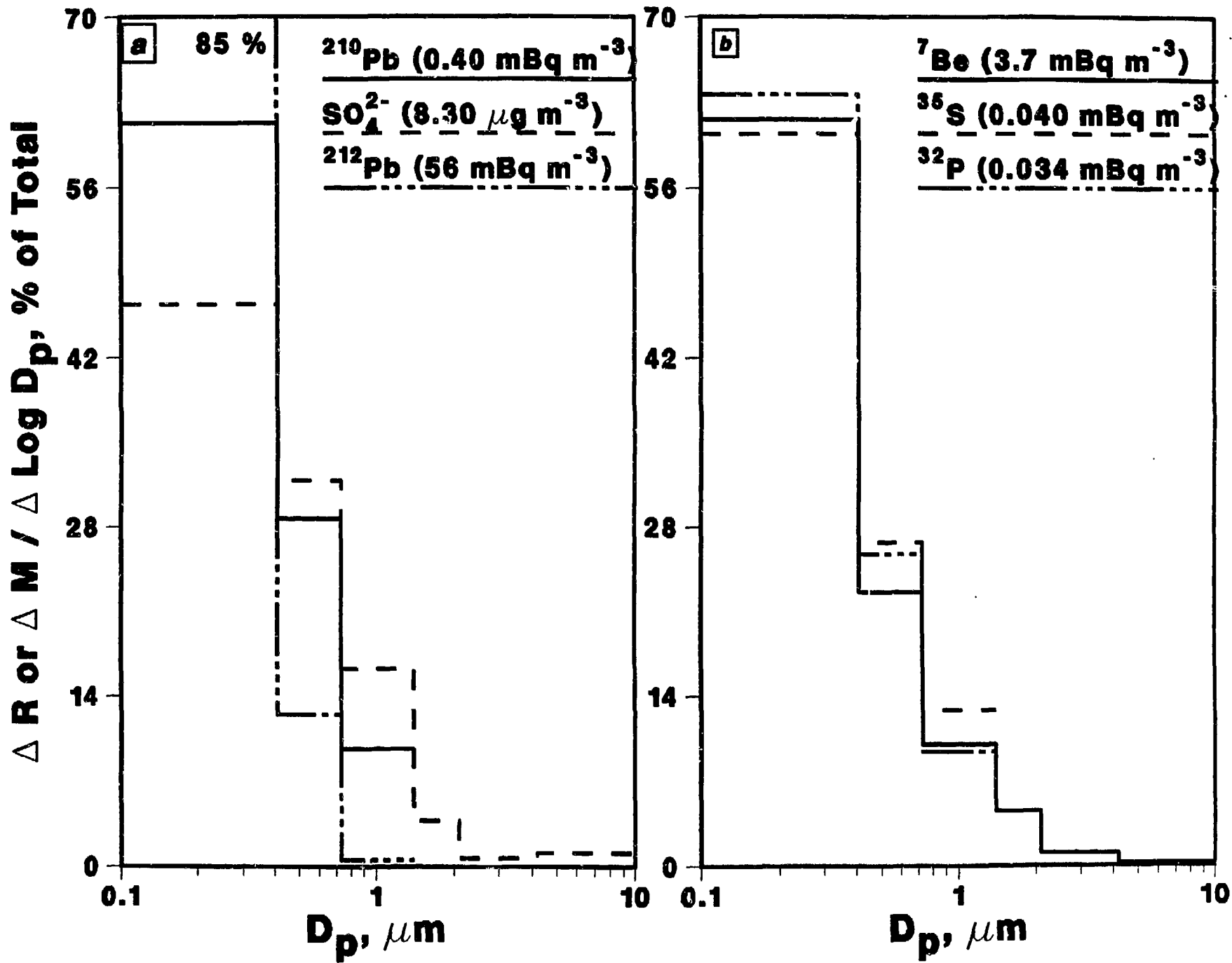
Acknowledgments

FIGURES

Figure 1.   Representative plots from 46 low-pressure impactor measurements, illustrating aerodynamic size (D_p) distributions of Pb-212 and Pb-214 (R = radioactivity). (a) type results occurred 46% of the time, (b) 39% of the time, (c) 8.7% of the time, and (d) 6.5% of the time. Lower D_p limits are arbitrary.

Figure 2.   Aerodynamic size (D_p) distributions of Pb-212 and Pb-214 activity (R) found with 1-ACFM and high-volume (HVI) impactors illustrating the particle shift of Pb-214. Lower D_p limits are arbitrary.

Figure 3.   A comparison of mean Pb-212 activity (R), and SO_4^{2-} mass (M) aerodynamic size (D_p) distributions from low-pressure impactor measurements made between Feb. and Sept. 1985. Lower D_p limits are arbitrary.

Figure 4.   Aerodynamic size (D_p) distributions of radionuclides (R) and SO_4^{2} (M) derived from a 7-d sampling (Feb. 1986) made using two high-volume cascade impactors. Pb-212, S-35, P-32, and Pb-210 were only measured on three stages (< 1.4 μm). Lower D_p limits are arbitrary.

Figure 5.   Results of an empirical model that calculated, for each low-pressure impactor size range, the percentage recoil losses of Pb-214 [subplot (a)] necessary to produce a calculated Pb-214 distribution is best agreement with the observed distribution [subplot (b)]. Lower D_p limits are arbitrary.
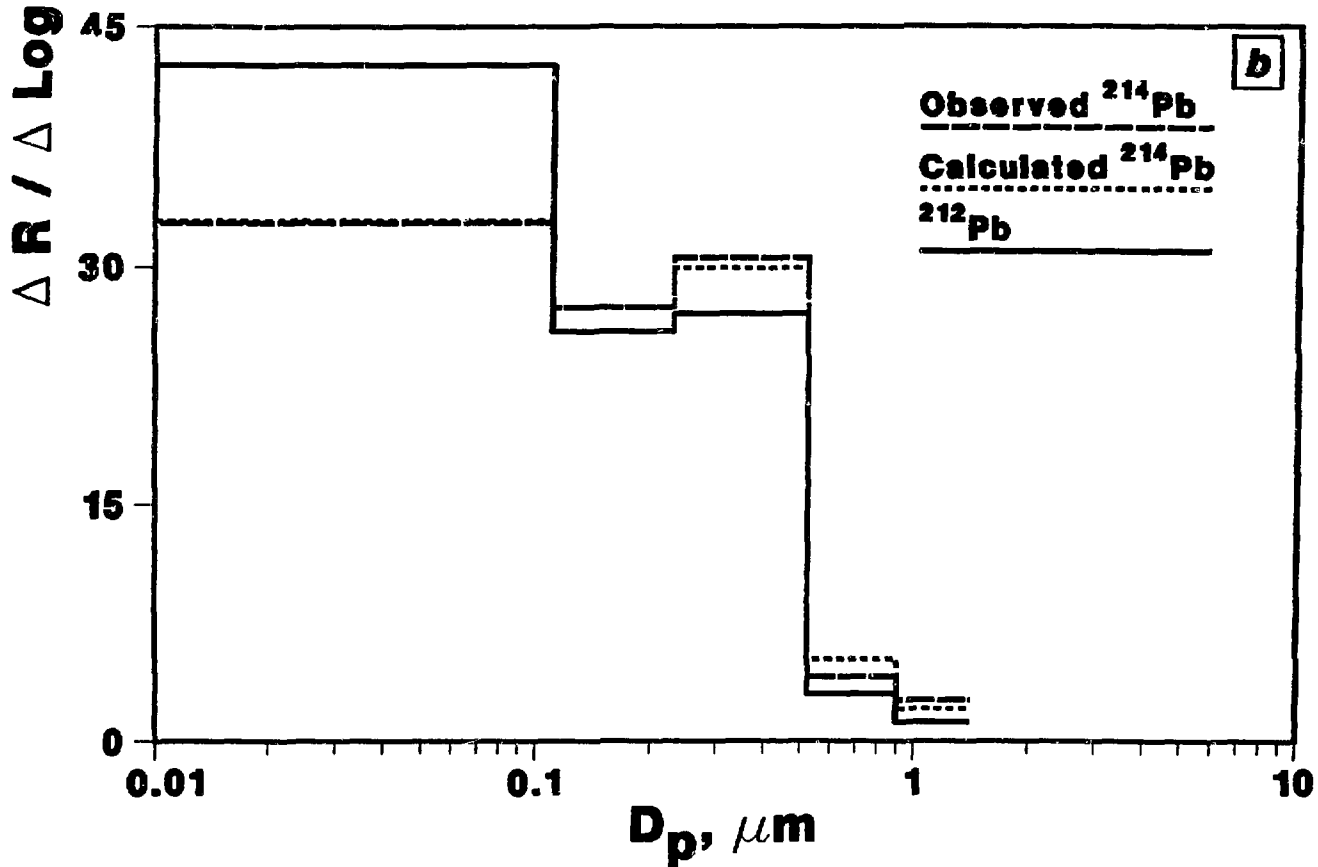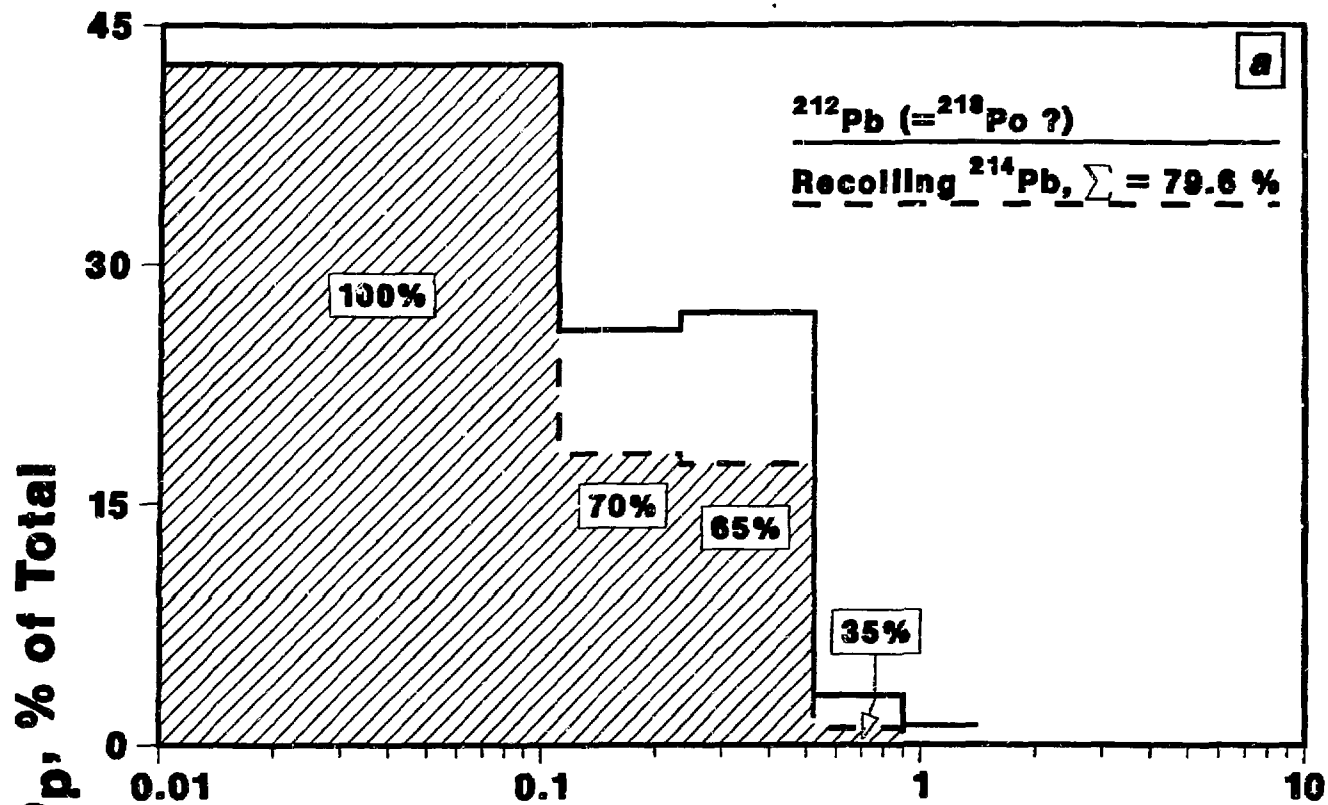
ORNL–DWG 86-1785

ORNL–DWG 86-1788

^{212}Pb (N=32)

SO_4^{2-} (N=12; 11.0 $\mu g\ m^{-3}$)

AMAD = 0.13 μm

MMAD = 0.38 μm

D_p, μm

Δ R or Δ M / Δ Log D_p, % Of Total

a

^{212}Pb (=^{218}Po ?)

Recoiling ^{214}Pb, $\sum$ = 79.6 %

100%

70%

65%

35%

b

Observed ^{214}Pb

Calculated ^{214}Pb

^{212}Pb

$\Delta R / \Delta \log D_p$, % of Total

D_p, μm

Fig 5
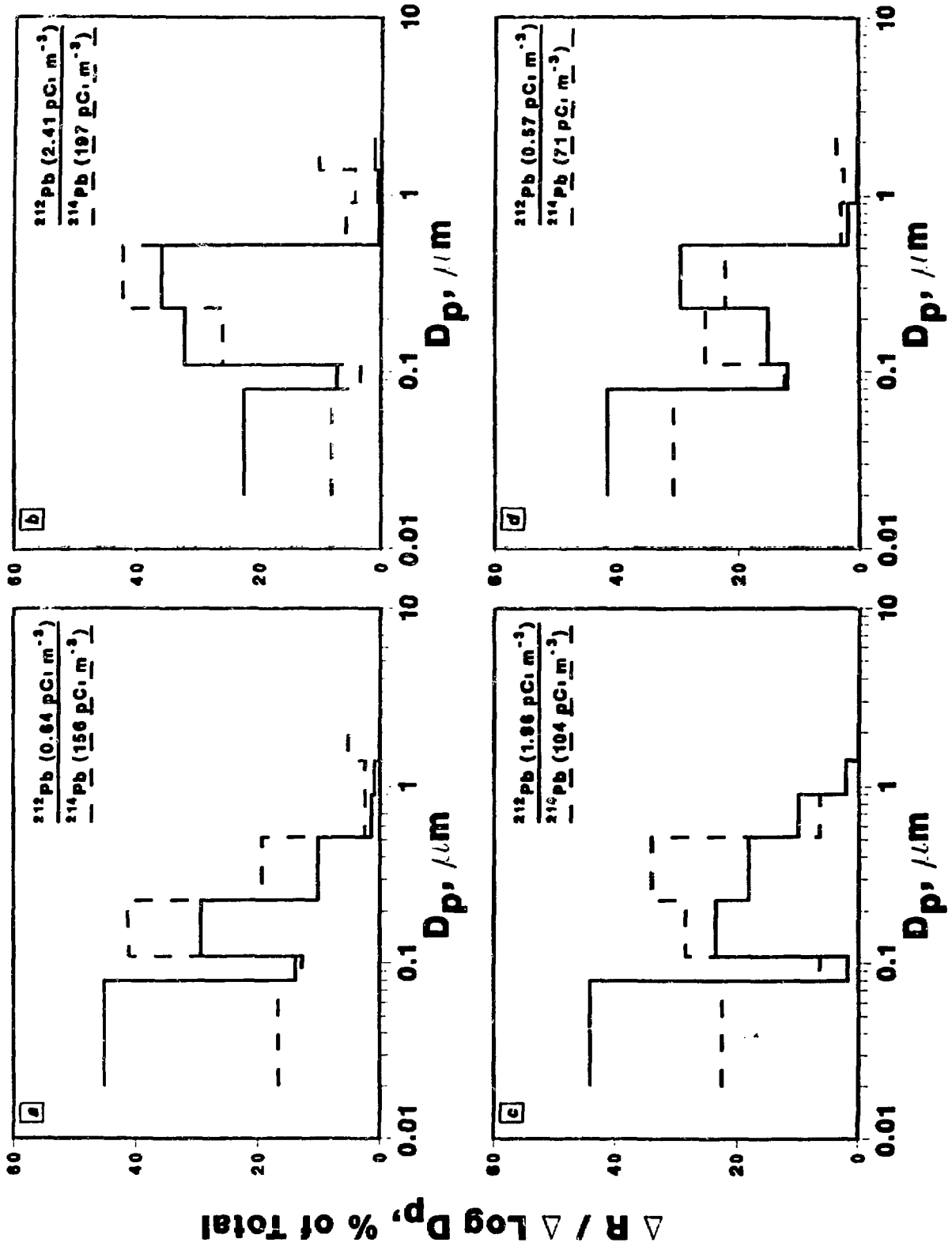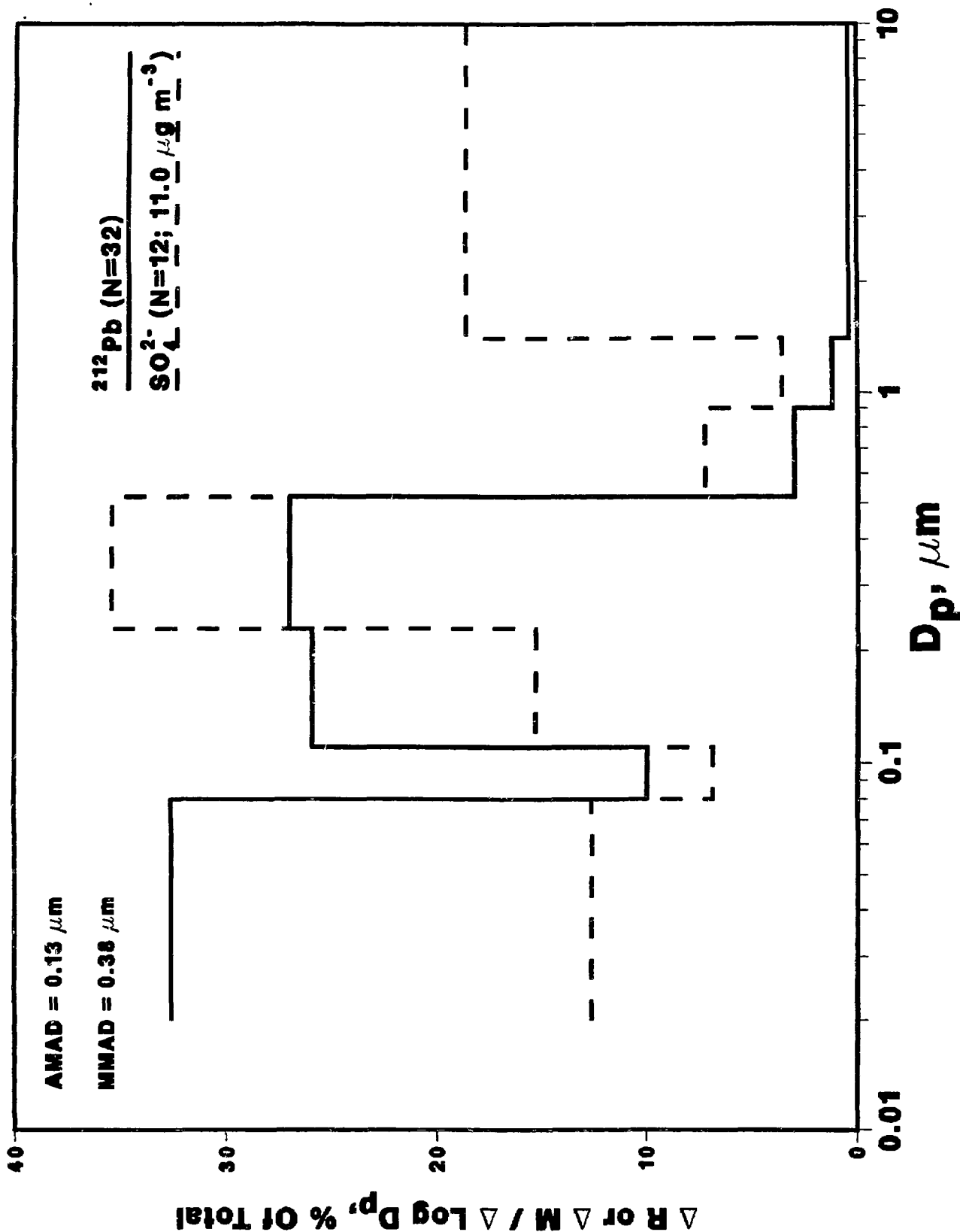
Table I. Mean Observed Pb-212 and Pb-214 Distributions and Frequency of Dominance

	≤ 0.08 μm	0.08–0.11 μm	0.11–0.23 μm	0.23–0.52 μm	0.52–0.9 μm	0.09–1.4 μm
	Distribution of 44 measurements (%)					
Pb-212	32.6	9.9	25.9	27.0	3.02	1.58
Pb-214	21.3	11.4	27.4	30.5	4.12	2.63
	Frequency of dominance (%)					
Pb-214	28.2	52.2	65.2	58.7	73.9	71.7
Pb-212	69.6	47.8	34.8	41.3	23.9	23.9
Equal	2.2	0	0	0	2.2	4.4

Table II. Summary of Mean Monthly Activity Median Aerodynamic Diameters (AMAD) and Geometric Standard Deviations (σ_g) of Radon and Thoron Daughter Size Distributions in Ambient Aerosols

Period (month)	Number of samples	Pb-214		Pb-212	
		AMAD (μm)	σ_g	AMAD (μm)	σ_g
December 1984	2	0.16	2.35	0.15	2.80
January 1985	2	0.17	2.46	0.09	2.96
March	5	0.17	2.33	0.12	2.46
April	5	0.18	2.08	0.17	2.25
May	3	0.20	2.28	0.20	2.35
June 7	4	0.21	2.98	0.17	2.38
July	6	0.16	3.27	0.23	3.52
August	6	0.12	32.51	0.10	3.11
September	10	0.13	3.68	0.11	3.44
October	2	0.09	3.13	0.09	2.85
November	1	0.07	3.20	0.12	6.70
December	2	NR*	NR*	0.13	4.35

*NR = not recorded.

Table III.   Median Aerodynamic Diameters (MAD) and Geometric Standard
              Deviations (σ_g) of Pb-210 and Be-7 Based on
              Radioactivity and SO_4^{2-} Measured with High-Volume
              Cascade Impactors

Month	MAD, μm ($\pm\sigma_g$)		
	Pb-210	Be-7	SO_4^{2-}
June 1985	–	0.50 (2.3)	0.50 (1.80)
July #1	0.49 (1.8)	0.30 (3.5)	0.49 (1.8)
July #2	–	0.31 (2.7)	0.38 (2.0)
July #3	–	0.48 (2.1)	0.48 (2.1)
August #1	0.40 (2.0)	0.36 (2.5)	0.41 (2.2)
August #2	0.40 (1.9)	0.30 (2.2)	0.40 (1.9)
September	–	0.34 (2.2)	0.45 (2.3)
November	–	0.34 (2.2)	0.45 (2.3)
December	–	0.32 (2.5)	0.58 (2.5)
January #1, 1986	–	0.32 (2.6)	0.42 (2.3)
January #2	0.32 (2.1)	–	–
February #1	0.32 (2.0)	–	–
February #2	0.36 (1.8)	0.34 (2.3)	0.43 (2.1)
March #1	0.28 (1.6)	0.32 (2.5)	–
March #2	–	0.29 (2.2)	0.41 (2.1)